12th International Conference on Fracture Mechanics of Concrete and Concrete Structures
FraMCoS-12
B.L.A. Pichler, Ch. Hellmich, P. Preinstorfer (Eds)

https://doi.org/10.21012/FC12.1270
MS06-2:3

EFFECT OF FIBER ALIGNMENT ON THE MECHANICAL AND ELECTRICAL PROPERTIES OF CARBON FIBER REINFORCED CEMENT COMPOSITE

S.F. QIN[*], N. LIU[†] AND J.S. QIU[†]

[*, †] The Hong Kong University of Science and Technology, Department of Civil and Environmental Engineering
Clear Water Bay, Hong Kong, China
e-mail: sqinae@connect.ust.hk, https://hkust.edu.hk/

Key words: Carbon Fiber, Fiber Reinforced Cementitious Composite, Fiber Alignment, Flexural, Electrical resistance.

Abstract: In previous research, the utilization of carbon fibers in composite materials has garnered significant attention due to their exceptional mechanical and electrical properties. One promising method for optimizing these properties is through the control of fiber orientation during the extrusion-based 3D printing process. In this study, the orientation of long carbon fibers, specifically measuring 6 mm and 12 mm in length, was successfully controlled using extrusion-based 3D printing techniques via a syringe. The investigation focused on the effects of fiber aspect ratio, volume fraction, and orientation on the electrical properties of the carbon fiber reinforced cementitious composites (c-FRCC) under three-point bending conditions. Flexural hardening was enhanced by the controlled fiber alignment. Electrical results reveal that the electrical resistance (R) of all specimens with aligned carbon fibers is more sensitive to flexural deflection than that of specimens with random fiber orientation before localized failure. The sensitivity in the fractional change in electrical resistance, $(R\text{-}R_0)/R_0$, improved with increasing aspect ratio and volume fraction of carbon fibers. Understanding these relationships is essential for developing advanced materials with tailored properties for crack self-sensing.

1 INTRODUCTION

The addition of fiber can enhance the mechanical performance of cement-based composites [1]. The improved mechanical performance has been shown to be influenced by fiber-related parameters, including fiber aspect ratio, volume fraction, fiber type, and fiber/interface bonding capacity [2]. Moreover, fiber orientation is a critical factor that significantly determines the mechanical properties, with fiber alignment being adjustable through the rheology of the cement-based matrix and achieved via specific extrusion molding [3-5]. For steel fibers, electromagnetic control of fiber orientation has also been reported [6].

In contrast to steel fibers and flexible fibers (e.g., PP, PE, or PVA fibers), there has been limited research on the control of fiber alignment for carbon fibers. Rutzen et al. achieved specific fiber alignment control by utilizing a syringe with a nozzle whose exit size is smaller than the length of the carbon fibers [7]. The flexural strength was enhanced, reaching up to 120 MPa with relatively higher strain by extruding 1-3 vol.% of 3-mm length carbon fibers. However, no further investigations have been conducted on the effect of fiber orientation while considering other parameters of carbon fibers, such as aspect ratio and bonding capacity.

Another advantage of utilizing carbon fibers is their stable electrical conductivity [1], unlike steel fibers, whose conductivity is easily affected by steel passivation under

alkaline cement conditions [8, 9]. This stable electrical property enables carbon fiber-cement composites to exhibit a electrical response to loading stimuli (referred to as piezoelectricity), which primarily depends on the types of electrical fillers, their shape, aspect ratio, and volume fraction of the carbon fibers [10]. However, the effect of aligned carbon fibers on the piezoelectric properties of carbon fiber-reinforced cementitious composites has not received sufficient attention. Specific fiber orientation enhances mechanical performance while forming specific electrical networks compared to randomly percolated carbon fibers [11].

In this study, the orientation of long carbon fibers was controlled through extrusion-based 3D printing using a syringe. The effects of aspect ratio, volume fraction, and orientation of carbon fibers on the electrical properties of c-FRCC under three-point bending were investigated.

2 MATERIALS AND METHODS

2.1 Materials

CEM I 52.5 Portland Cement was procured from Green Island Cement Co., Ltd (Hong Kong, China). Fly ash was generated by a local power plant in Castle Peak (Hong Kong, China). Highly active micro-silica fume was from Elkem Co., Ltd (China). The physical characteristics of chopped polyacrylonitrile (PAN)-based carbon fiber (CF) purchased from Toho Tenax Co., Ltd. Tokyo, Japan are listed in **Table 1**. Besides, a kind of polycarboxylate-type polymer superplasticizer (Sp.) (ADVA® 189, Grace Co., Ltd, America) was used in this study.

Table 1: Physical properties of CFs in this study

Properties	CF
Length (mm)	6 or 12
Diameter (μm)	7
Tensile strength (MPa)	4900
Young's modulus (GPa)	230
Conductivity (kS/m)	64.6±2.1
Density (specific gravity, g/cm3)	1.75

2.2 Preparation of c-FRCC specimen

The mix designs of fiber-cement composite are listed in **Table 2**. The naming rule is based on the length of CF and the volume fraction added to the cement matrix. Specifically, the water-to-cement ratio was 0.26. Besides, the cement/binders (cement and fly ash) ratio were 0.26 for the group with 0.5 vol. % of the CFs, while 3 wt.% replacement of fly ash by silica fume was added to improve the rheology of the composites in the case of groups with 1.0 vol. % of the CFs. Cement and fly ash (or with silica fume) were first mixed for about 5 mins. At the same time, the superplasticizer was mixed in the water before they were added to the mixed raw materials for 3 mins. After that, CFs were added to the cement paste and mixed for 5 mins.

After that, a part of the as-prepared fiber-cement composite was then placed in an injector, as presented in **Figure 1a**, for the extrusion-based 3D printing with the specific route presented in **Figure 1b**. The extrusion-based 3D printing used in the study was designed based on a commercialized 3D printer (MOORE 1, TRONXY Co., Ltd, Shenzhen, China) equipped with a 100 ml injector. It is reported that the 3D printing technique was applied to control the fiber orientation to a large degree [7]. It should be noted that the as-prepared composite was under continuous slow-speedy stirring when the 3D printing was proceeding, avoiding the initial setting. Besides, the extrusion speed was set as the same to the printing moving speed, reducing the adverse effect on the fiber distribution and alignment [11]. When the printing moving speed is larger, the extruded composite will be elongated, while the lower will result in the compaction of the composite and the mold. The dimension of the fiber-cement composite was according to the standard (ASTM D7264/D7264M−07).

Table 3 summarizes the as-prepared groups with varying factors, such as the length of CFs (6 mm or 12 mm), the volume fraction of CFs (0.5 vol.% or 1.0 vol.%), and the fiber orientation. As shown in **Figure 1b**, the four-

probe measurement regions of the specimen were designed with random (R) and longitudinal (L) fiber alignment of CFs (i.e., RCF and LCF groups). After 28 days of hydration under the standard condition (95% humidity, 25°C), the upper surface of the as-prepared samples was polished till the thickness of the sample was around 3.1 ± 0.05 mm. After cleaning and drying under room conditions, the surface at the tension side of the specimen was painted with conductive silver paint before the copper tape was attached to the position, as shown in Figure 1b. Four-probe measurement was performed to obtain the electrical resistance in the following section. Besides, two types of testing samples were prepared with/without notches on the mid-span (the width of the notches is 0.5 mm). The creation of the notches makes sure the localized crack occurs on the mid-span, while the traditional notch created at the bottom of the specimen results in the non-uniform current flow at the compression and tension zones. In the absence of notches, the crack propagation is able to be realized during the three-point bending testing.

Table 2: Mix design of the carbon fiber-cement composite.

Groups	Length (mm)	CF (vol.%)	Cement (g/L)	Fly ash (g/L)	Silica Fume (g/L)	Water (g/L)	Sp. (g/L)
6-CF05	6	0.5	402	1127		397	2
12-CF05	12	0.5	402	1127		397	2
12-CF10	12	10	402	1086	33.6	397	3.8

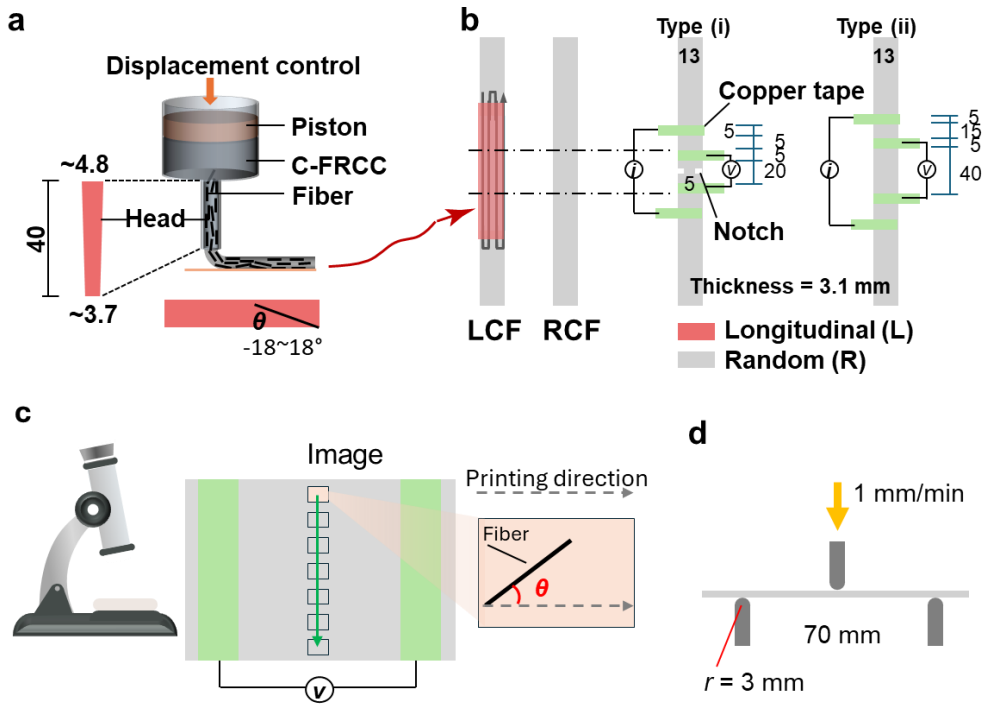

Figure 1. Illustrations of the experimental section (a) the fiber alignment control by the extrusion injector with the relevant size of the head, (b) the printing route for preparing fiber-cement composite with the controllable fiber alignment and dimension, (c) fiber orientation analysis via microscopy measurement and image process, and (d) three-point bending setup with dimension.

Table 3: Statistical analysis of fiber orientation, initial resistance and the ultimate flexural strength.

Specimen	Group	Percentage (-18°~18°)	R's square (R^2)	Resistance (Ω) (±error)	Strength (MPa) (±error)
Type (i)	Ref.	N/A	N/A	344k (±7.1k)	4.39 (±0.19)
Type (i)	R6-CF05	21.6%	0.500	39.48 (±6.71)	19.49 (±6.66)
	L6-CF05	56.0%	0.800	55.01 (±3.81)	18.17 (±4.09)
	R12-CF05	45.3%	0.810	23.62 (±1.68)	14.74 (±1.87)
	L12-CF05	73.6%	0.958	28.46 (±4.67)	23.52 (±3.35)
	R12-CF10	17.0%	0.610	31.3 (±1.02)	26.74 (±7.48)
	L12-CF10	63.6%	0.942	27.59 (±3.54)	38.04 (±2.70)
Type (ii)	R12-CF05	30.7%	0.751	19.37 (±1.78)	18.60 (±1.86)
	L12-CF05	69.3%	0.964	20.30 (±2.25)	26.54 (±4.66)

2.3 Fiber orientation analysis

Optical microscopy with a minimum magnification (5x) was applied to capture the fiber distribution on the upper surface of the fiber-cement composite, as presented in **Figure 1c**. About 15 surface images of each specimen were collected, and the fiber orientation angle (θ) of each fiber was then measured via ImageJ Fuji software. Three parallel samples for each group were recorded, and the standard Gaussian curve was then used to fit the sum of the angles in each group to analyze the fiber orientation of the RCF and LCF groups.

2.4 Electrical resistance measurement under three-point bending

A three-point bending ramping testing was performed using the loading machine (Lloyd Instruments EZ50, Ametek, America) equipped with a 50 N load cell, as presented in **Figure 1d**. The loading rate was 1 mm/min, and the span-to-thickness ratio was about 22.5, according to ASTM D7264/D7264M−07 standard. Therefore, the flexural strength (σ_f) can be obtained by the following equation,

$$\sigma_f = 3FL/(2bd\text{^}2) \quad (1)$$

where ***F*** is a load at a given point on the load-deflection curve (N), ***L*** is the support span (7 mm), ***b*** is the width of the midspan (13 mm) and ***d*** is the thickness of the tested midspan.

The electrical resistance was synchronously recorded during the mechanical testing via an electrical workstation (SP-200 workstation, Biologic, France). The application of the four-probe measurement enables to compromise the effect of connection from the copper electrode to the composite to a large extent. In the study, 0.1 V potential was performed, and the electrical current was recorded with a frequency of 5 Hz. Thus, the fractional change in the resistance [$(R-R_0)/R_0$] was then obtained through Eq. (2),

$$(R-R_0)/R_0 = (i_0/i-1) \times 100\% \quad (2)$$

where i_0 is the initial current without loading and i is the current as the flection changes.

3 RESULTS AND DISCUSSIONS

Figure 2 presents the result of the fiber orientations for LCF and RCF groups (12 mm length and 0.5 vol.%). High R's square indicates the fiber orientations were successfully controlled by the extrusion-based 3D printing technique. Ideally, the permissible angle (θ) range between fiber orientation and printing direction is ideally within ±18° due to the injector head size limitation when comparing the length of 12-mm long CF. The cumulative percentage of the L12-CF05 group within ±18° remains 70%. **Table 3** also summarizes the fitting results and the ratio of all the groups. Short fiber allows more random fiber orientation, leading to a lower percentage with lower R's square (see **Table 3**). Besides, the average resistance of all the specimens is listed in **Table 3**. With carbon fibers, the electrical resistance decreased significantly,

and the decline degree in the resistance relies on the aspect ratio and the volume fraction of carbon fibers [10]. The presence of the notches compromises the electrical conduction network, resulting in higher resistance.

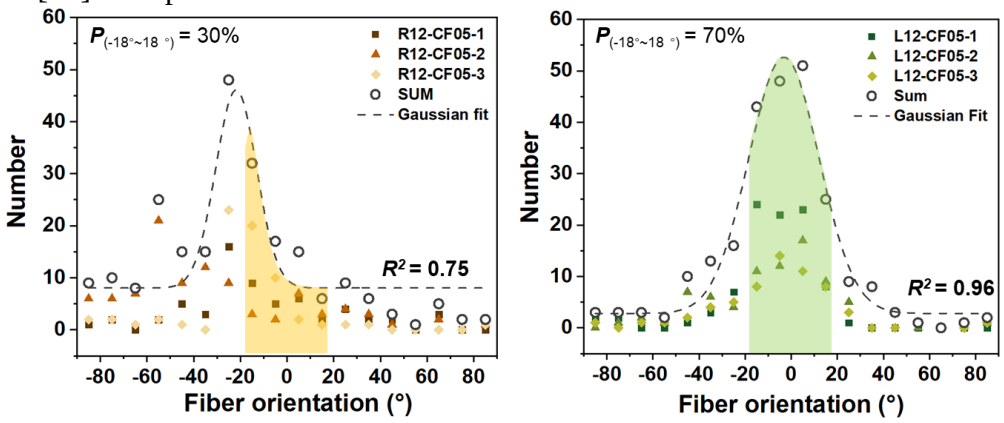

Figure 2. The statistical results of fiber orientation, and the highligted region is the probability of the fiber orientation within ±18°.

Figure 3 shows the characteristics of flexural and electrical behaviors for different groups with notches. The average flexural strength is summarized in **Table 3**. The incorporation of carbon fiber enhances the flexural strength that was improved by the larger aspect ratio, the increasing volume fraction, and the better fiber alignment along with loading direction. With notches, deflection hardening was not observed. As for electrical resistance, the resistance is not sensitive to deflection in the elastic stage. In our previous study [12], we found that the advantage of fiber orientation in the elastic stage is not obvious in the elastic stage. However, in the plastic stage before cracking, the resistance of the sample with oriented carbon fiber arrangement is more sensitive to deflection. After localized cracking, the resistance varied with the increasing deflection.

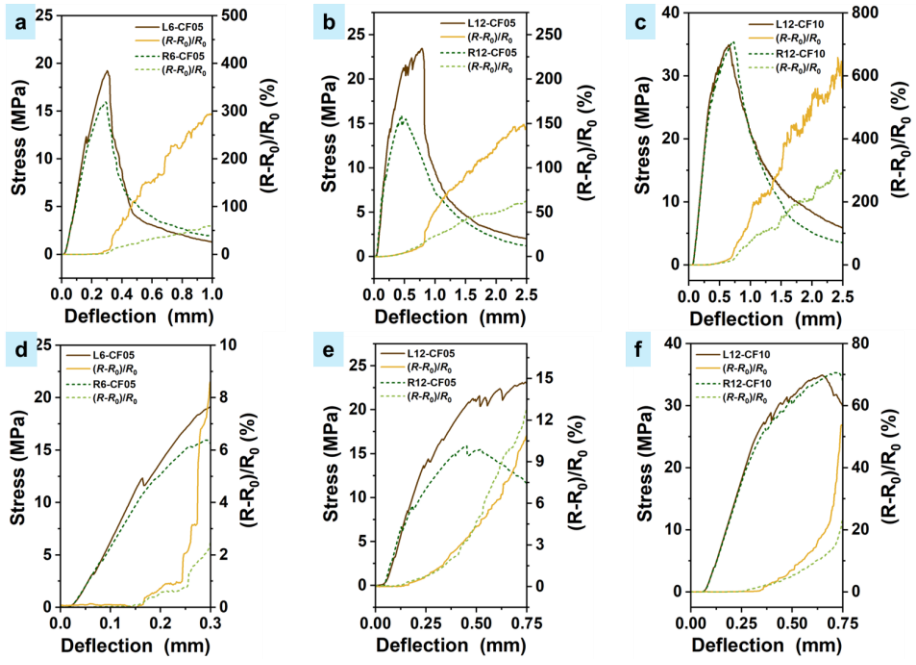

Figure 3. The characteristics results of flexural and electrical behavior for type (i) groups: (a) 6-CF05, (b) 12-CF05, (c) 12-CF10; (d)(e)(f) the corresponding magnified results before localized cracking.

Figure 4 summarizes the flexural strength of all type (i) groups and the fractional change in the electrical resistance at localized cracking for all type (i) specimens. In brief, LCF groups present higher sensitivity than RCF groups but with higher deviation. Such an enhancement is related to the increasing fiber aspect ratio and fiber volume fraction.

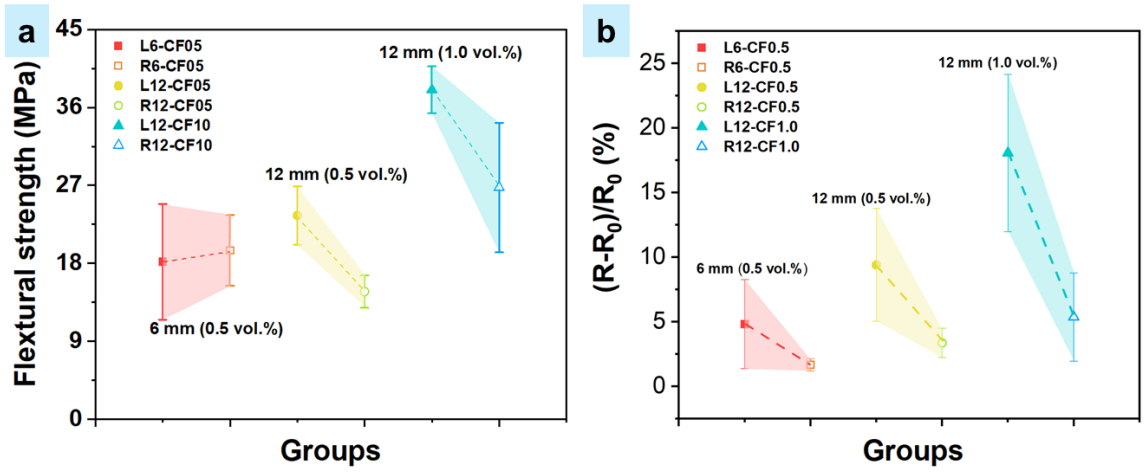

Figure 4. (a) the flexural strength and (b) the fractional change in the electrical resistance at the localized cracking for type (i) groups.

Figure 5 describes the flexural and electrical behaviors of the type (ii) specimens. The stress-deflection curve was divided into three stages, i.e., the linear elastic stage, first cracking and crack propagation stage, and localized cracking or failure stage. In the first stage, the fraction change in the resistance did not increase significantly till the occurrence of the first crack at the endpoint of the stage. In the second stage, obvious deflection-hardening can be observed, and the hardening efficiency of the L12-CF05 was better than the R12-CF05 group. One of the RCF specimens presents a higher hardening probably due to the random fiber orientation at the midspan being similar to the LCF one. Interestingly, the electrical resistance of all LCF specimens is more highly sensitive to deflection when compared to the RCF specimen which showed higher stability of the $(R\text{-}R_0)/R_0$ versus deflection. Such stability of the RCF group still appeared in the third stage, while the LCF group became less sensitive and stable to the increasing deflection.

Previous research has shown that fiber orientation significantly affects mechanical behaviors, i.e., tensile and flexural strength [5,7]. The tailored fiber orientation by the extrusion-based enhanced the strain hardening [5] and deflection-hardening [7] and. In their studies, the former utilized 1.0 vol.% of 3-mm length carbon fibers in the cement/silica fume matrix, while the latter investigated the effect of aligned 1.0 vol.% of 12-mm PVA and PE fibers on the tensile behavior in the cement/fly ash matrix. The participating carbon fibers enable electrical conduction, while longer fiber improves strain-hardening in the cement/fly ash system. In our experiment, only 0.5 vol.% of 12-mm carbon fiber was used to achieve the higher deflection hardening, which is larger than the case with 1.0 vol.% of 3-mm length carbon fibers in the cement/silica fume matrix [7], as shown in **Table** 4.

Table 4: Flexural strain at the first cracking and the localized cracking.

Strain	#1 (%)	#2 (%)	#2 - #1(%)
L12-CF05	1.23	8.47	7.24
	1.57	8.06	6.50
	1.58	10.16	8.58
R12-CF05	1.48	5.18	3.71
	1.54	9.40	7.86
	1.44	6.47	5.03

Strain #1 is the strain at first cracking in Fig.5.
Strain #2 is the strain at the localized cracking.

Such a phenomenon was related to the mix design with higher ratio of fly ash which allows fiber-bridging crack propagation after first cracking due to weaker binding capacity between the carbon fiber and the cementitious matrix. The bridging fibers may go through debonding, slippage and rupture against the matrix, which mainly depends on the matrix type (that affect chemical bonding and friction stress between the fiber and cement matrix), and fiber orientation.

Besides, the electrical resistance presented a higher sensitivity to the deflection before localized failure, especially for the LCF group, despite the fact that the RCF group exhibited more stable electrical signals before and after localized failure. After the localized failure, randomly aligned fibers easily rupture due to the variable direction that differs from the load direction at the tension side, and it leads to the increase in the resistance. On the contrary, longitudinal-aligned fibers are close to the tension direction, and more bridged fibers provide electrical channels for electron conduction.

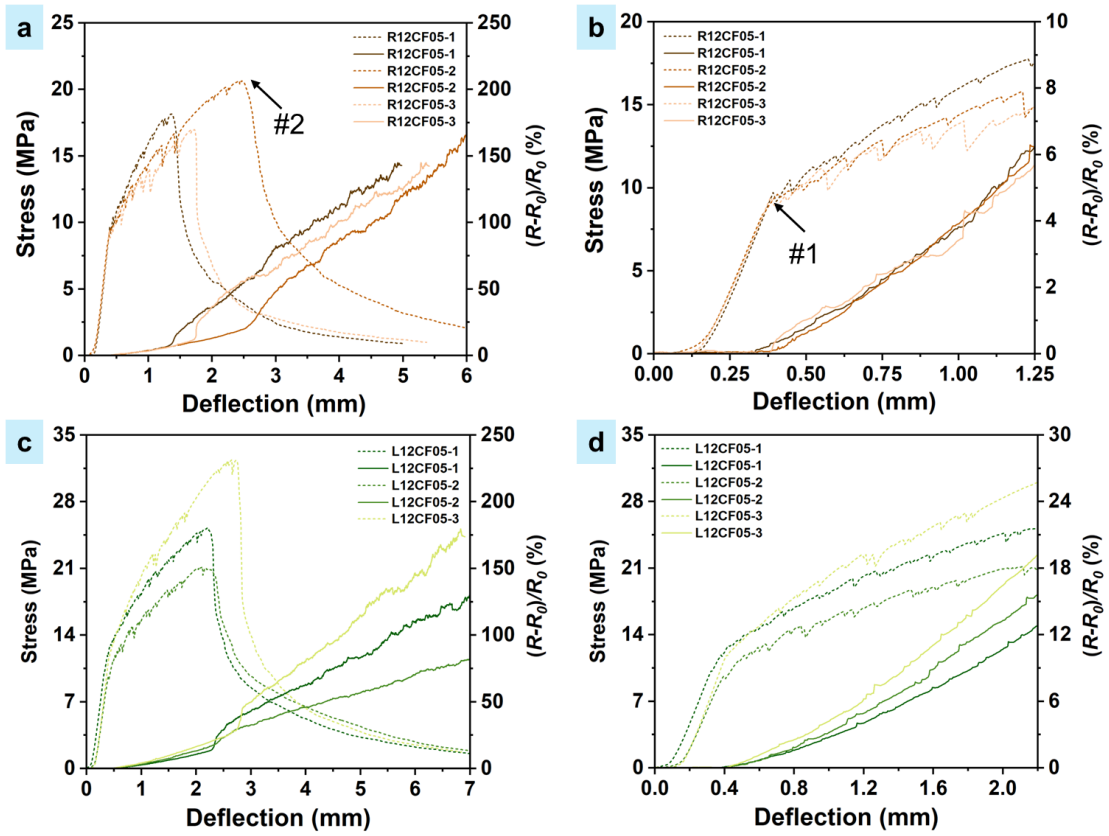

Figure 5. Mechanical and electrical behaviors for type (ii) groups: (a) R12-CF05 group with (b) the corresponding magnified results before the localized failure, (c) L12-CF05 group with (D) the corresponding magnified results before the localized failure.

4 CONCLUSIONS

The orientation of carbon fibers can be controlled in the cementitious composite with high fly ash content by using the extrusion-based 3D printing technique through a nozzle. 60%-70% of long carbon fibers in any given group can be aligned. The flexural strength of specimen with longitudinal aligned fibers reaches up to 15-40 MPa, which is more than 3 times that of the Ref. sample without fiber reinforcement. The longer carbon fiber allows more significant enhancements when compared LCF with RCF group.

Before localized failure, all LCF groups present higher sensitivity to the deflection

under three-point bending, and the improvement relies on the increasing aspect ratio and volume fraction of carbon fibers. However, the RCF group demonstrated more stable electrical signals after the localized cracking. These potential relationships between mechanical and electrical behaviors related to the micromechanics of the carbon fibers in the matrix (probably like fiber debonding, slippage and rupture).

REFERENCES

[1] Chen, P.W. and Chung, D.D.L., 1996. Concrete as a new strain stress sensor. *Composites Part B-Engineering*. **27**: 11-23.

[2] Li, J., Qiu, J., Weng, J. and Yang, E.-H., 2023. Micromechanics of engineered cementitious composites (ECC): A critical review and new insights. *Construction and Building Materials*. **362**: 129765.

[3] Huang, H., Gao, X., Li, L. and Wang, H., 2018. Improvement effect of steel fiber orientation control on mechanical performance of UHPC. *Construction and Building Materials*. **188**: 709-721.

[4] Arunothayan, A.R., Nematollahi, B., Ranade, R., Bong, S.H., Sanjayan, J.G. and Khayat, K.H., 2021. Fiber orientation effects on ultra-high performance concrete formed by 3D printing. *Cement and Concrete Research*. **143**: 106384.

[5] Curosu, I., Muja, E., Ismailov, M., Ahmed, A.H., Liebscher, M. and Mechtcherine, V., 2022. An experimental-analytical scale-linking study on the crack-bridging mechanisms in different types of SHCC in dependence on fiber orientation. *Cement and Concrete Research*. **152**: 106650.

[6] Mu, R., Li, H., Qing, L., Lin, J. and Zhao, Q., 2017. Aligning steel fibers in cement mortar using electro-magnetic field. *Construction and Building Materials*. **131**: 309-316.

[7] Rutzen, M., Lauff, P., Niedermeier, R., Fischer, O., Raith, M., Grosse, C.U., Weiss, U., Peter, M.A. and Volkmer, D., 2021. Influence of fiber alignment on pseudoductility and microcracking in a cementitious carbon fiber composite material. *Materials and Structures*. **54**: 1-21.

[8] Fu, X. and Chung, D., 1996. Single-fiber electromechanical pull-out testing and its application to studying the interface between steel fiber and cement. *Composite Interfaces*. **4**: 197-211.

[9] Torrents, J.M., Mason, T.O., Peled, A., Shah, S.P. and Garboczi, E.J., 2001. Analysis of the impedance spectra of short conductive fiber-reinforced composites. *Journal of Materials Science*. **36**: 4003-4012.

[10] Dong, W., Li, W., Tao, Z. and Wang, K., 2019. Piezoresistive properties of cement-based sensors: Review and perspective. *Construction and Building Materials*. **203**: 146-163.

[11] Wright, W.J. and Celik, E., 2023. In Situ Electrical Network Activation and Deactivation in Short Carbon Fiber Composites via 3D Printing. *Advanced Functional Materials*. **33**: 2303282.

[12] Qin, S., Liu, N. and Qiu, J., 2024. The effect of controlled fiber alignment of carbon fibers on the electrical properties of carbon fiber-cement composite under cyclic flexural loading. *Procedia Structural Integrity*. **64**: 168-174.